nature climate change

LETTERS

https://doi.org/10.1038/s41558-017-0020-x

The far reach of ice-shelf thinning in Antarctica

R. Reese[1,2], G. H. Gudmundsson[3], A. Levermann[1,2,4] and R. Winkelmann[1,2*]

Floating ice shelves, which fringe most of Antarctica's coastline, regulate ice flow into the Southern Ocean[1–3]. Their thinning[4–7] or disintegration[8,9] can cause upstream acceleration of grounded ice and raise global sea levels. So far the effect has not been quantified in a comprehensive and spatially explicit manner. Here, using a finite-element model, we diagnose the immediate, continent-wide flux response to different spatial patterns of ice-shelf mass loss. We show that highly localized ice-shelf thinning can reach across the entire shelf and accelerate ice flow in regions far from the initial perturbation. As an example, this 'tele-buttressing' enhances outflow from Bindschadler Ice Stream in response to thinning near Ross Island more than 900 km away. We further find that the integrated flux response across all grounding lines is highly dependent on the location of imposed changes: the strongest response is caused not only near ice streams and ice rises, but also by thinning, for instance, well-within the Filchner–Ronne and Ross Ice Shelves. The most critical regions in all major ice shelves are often located in regions easily accessible to the intrusion of warm ocean waters[10–12], stressing Antarctica's vulnerability to changes in its surrounding ocean.

Owing to their ability to regulate upstream ice flow, Antarctic ice shelves play a key part in future sea-level rise in a warming world[5,13,14]. At the same time, as they are in direct contact with the ocean at their base and have low surface elevation, they are particularly vulnerable to a changing climate[15–19]. Ocean-induced thinning of ice shelves, which has been accelerating over the past decades[4], has the potential to reduce the restraining stress to ice sheet flow provided by ice shelves[1,2] and thereby enhance ice discharge across the grounding lines of the Antarctic Ice Sheet[6–9,20]. Although the importance of ice shelves in modulating ice flux from the interior of the Antarctic Ice Sheet across the grounding lines and into the ocean has been recognized for some time[21–24], no study has set out to systematically map the dependency of ice flux across the grounding lines to different spatial patterns of ice-shelf thinning.

By modifying the stress balance along the grounding line, ice shelves can 'buttress' the ice flow from the (grounded) ice sheet into the ocean. At any point along a grounding line ice-shelf buttressing can be quantified in terms of the impact that an ice shelf has on the state of stress compared to the state of stress in the hypothetical absence of the ice shelf[25]. Ice-shelf buttressing is primarily affected by how strongly the flow of an ice shelf is restricted both laterally and through local grounding (an unconfined ice shelf of uniform width provides no buttressing). However, it is also dependent on the geometry, thickness and rheological properties of the ice shelf[3,26,27]. Thinning in any part of a confined ice shelf affects the stress regime within the whole ice shelf, and therefore has the potential to impact the ice flux of all surrounding grounding lines. The impact of ice-shelf thinning on flow across grounding lines is expected to depend on a number of factors such as the location of thinning, how strongly the flow of the ice shelf is confined, ice flow properties upstream of the grounding lines, the ice softness and the shape of the grounding lines. Fully assessing the impact of ice-shelf thinning on the discharge from the Antarctic Ice Sheet therefore requires estimating the effect of thinning at any location on all grounding lines.

In order to identify the most critical ice shelf regions, we provide a comprehensive, quantitative assessment of the impact of any local ice-shelf thickness change on the discharge across the grounding lines of present-day Antarctica. Based on input inferred from data assimilation of present-day ice thickness[28] and velocities[29], we conduct a series of Antarctic-wide simulations with the finite-element model Úa[23], which solves for the ice flow in sheet and shelves simultaneously (using the shallow-shelf/shelfy-stream approximation of the momentum balance, see for example, refs [30,31]). At the ice front, the boundary condition is given by the vertically integrated, horizontal static fluid pressure of the ambient ocean. The grounding line position is diagnosed in Úa using the floatation criterion.

We express the effect of ice-shelf thinning as the ratio between the total changes in annual mass flux across all grounding lines to the magnitude of locally applied thinning (Fig. 1). In each diagnostic experiment, a 20 km × 20 km region is thinned by 1 m, and the immediate response in ice flux across all grounding lines determined. These perturbations mimic ice-shelf thinning patterns resulting from changes in ocean-induced melting. Idealized perturbations allow us to separate the contribution from different ice-shelf areas and therefore identify regions of particular importance for grounded ice loss. Subdividing the ice shelves into 20 km × 20 km sectors was found to be of sufficiently fine resolution to adequately resolve the spatial response pattern, and 1 m thinning sufficiently small to be within the linear response range (see Methods and Supplementary Figs. 1, 2). The impact of each local perturbation is then obtained by dividing the resulting increase in annual mass flux across all grounding lines R by the applied perturbation in ice shelf mass P. We refer to this non-dimensional ratio as the buttressing flux response number $\theta_B = R/P$ and express this number as a percentage. If, for example, $\theta_B = 100\%$, then the added annual mass flux across all grounding lines equals the mass-flux perturbation applied to the ice shelf, or 20 km × 20 km × 1 m × 910 kg m^{-3} = 0.364 Gt (assuming an ice density of 910 kg m^{-3}). Where the perturbed sector is crossed by part of the grounding line, the removed ice mass decreases accordingly. To ensure that the recorded flux response is only caused by changes in ice-shelf buttressing, and to exclude any potential impacts related to changes in driving stress over grounded regions, ice-shelf thinning is only applied to those elements of the computational grid that share no nodes with any elements crossing grounding lines (see Methods). With the buttressing flux

[1]Potsdam Institute for Climate Impact Research (PIK), Member of the Leibniz Association, PO Box 60 12 03, Potsdam, Germany. [2]Institute of Physics and Astronomy, University of Potsdam, Potsdam, Germany. [3]British Antarctic Survey, Cambridge, UK. [4]Lamont-Doherty Earth Observatory, Columbia University, New York, NY, USA. *e-mail: ricarda.winkelmann@pik-potsdam.de

© 2017 Macmillan Publishers Limited, part of Springer Nature. All rights reserved.

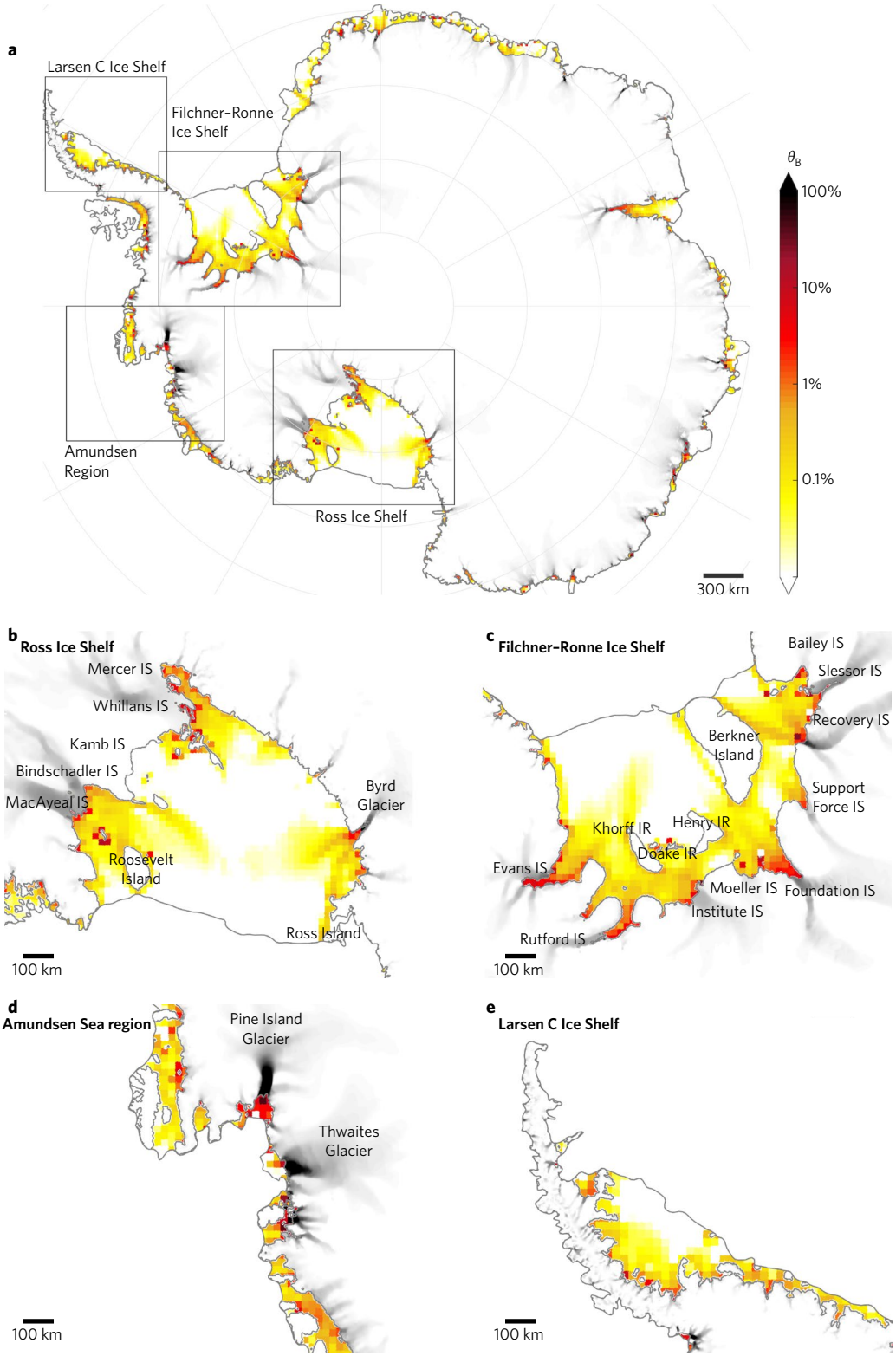

Fig. 1 | Buttressing flux response numbers (θ_B) for Antarctic ice shelves. At the location of each perturbation, the ratio of immediate change in ice flux across all grounding lines to the locally induced ice-shelf thinning is shown (expressed in percentages). As described in the Methods, the ice shelves are locally thinned by 1 m over areas of 20 km × 20 km. Grounding lines and ice front positions are indicated by grey lines. In grounded regions, ice speed is shown in grey, ranging up to 1,000 m per year. **a**, Antartic ice shelves. **b**–**e**, Enlargements of selected ice shelves shown in **a**. **b**, Ross Ice Shelf. **c**, Filchner–Ronne Ice Shelf. **d**, Amundsen Sea area. **e**, Larsen C Ice Shelf area. IR, ice rises; IS, ice streams.

response number θ_B we can therefore analyse the relative importance of different ice-shelf regions on the basis of their influence on the immediate flux change through shifts in the stress pattern.

Owing to the diagnostic approach, our analysis is based solely on present-day ice-shelf and ice-sheet conditions and is therefore independent of assumptions about changes in climatic boundary

© 2017 Macmillan Publishers Limited, part of Springer Nature. All rights reserved.

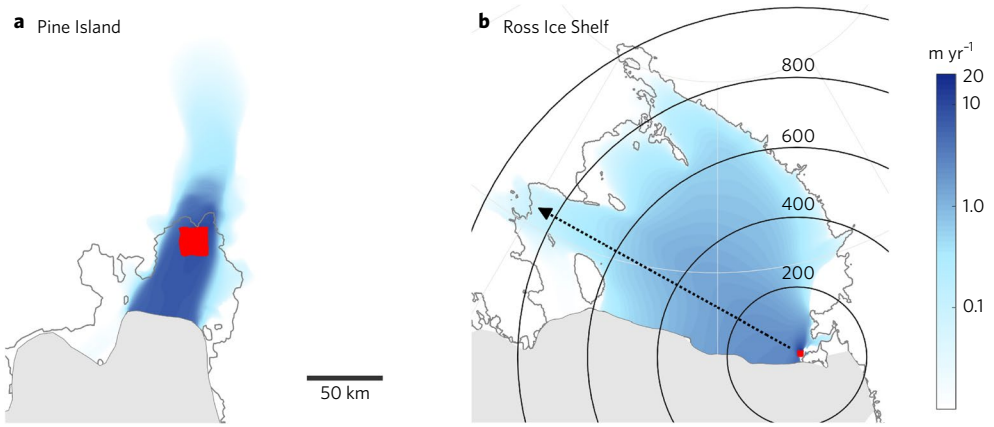

Fig. 2 | Examples of changes in speed resulting from 1 m thinning. a, Pine Island Glacier Ice Shelf. **b**, Ross Ice Shelf. The red squares indicate the area over which thinning is applied, the blue shading indicates the resulting change in ice flow speed. Ocean is shown in grey. **b**, The arrow gives an example for direction and the far-reaching impact of a local perturbation near Ross Island on the Bindschadler and MacAyeal ice streams (directions for all perturbation locations are given in the interaction matrices in Supplementary Figs. 3, 4). Black circles mark the distance from the perturbation location in 200 km contours (compare to Fig. 3b).

conditions. Modifications in ocean currents, for example, could induce changes in the patterns of sub-shelf melting. Combining our continent-wide map of the buttressing flux response number with observed or prognostic thinning patterns, we could assess the importance of any such observed changes.

We find the buttressing flux response number to be spatially highly variable (Fig. 1a). In general, the strongest response in integrated grounding line flux occurs for perturbations directly downstream of the grounding lines of fast-flowing glaciers and ice streams, but the magnitude of the individual responses differs significantly between ice streams. While ice-shelf margins are, as expected, crucial for the stress field and therefore for the induced flux changes, there are also areas well within the ice shelves with equally high response numbers (for example, within Filchner Ice Shelf). A region with a particularly high impact on upstream flow and ice flux across the grounding line is found directly downstream of Byrd Glacier (Fig. 1b), where the buttressing flux response number is 175%. Other critical areas with high θ_B values are found downstream of major ice streams, such as Mercer, Bindschadler and MacAyeal ice streams draining into Ross Ice Shelf, but not downstream of the stagnant Kamb Ice Stream, illustrating that the impact of ice-shelf thinning is dependent on mechanical conditions on both sides of the grounding line. For the Ronne-Filchner Ice Shelf, similarly critical areas are found downstream of Evans, Rutford and Foundation ice streams, and, to a lesser degree, downstream of Moeller Ice Stream (Fig. 1c). A very strong response is also found for the ice shelves adjacent to Pine-Island Glacier and other glaciers in the Amundsen region (Fig. 1d). In Larsen C Ice Shelf, the buttressing flux response number shows a similar pattern as in Filchner–Ronne and Ross ice shelves, with higher values along the grounding lines, especially near ice streams, and a decrease in θ_B towards the ice shelf front (Fig. 1e).

Ice rises and rumples provide a substantial source of buttressing[22,27], and our results confirm that ice thickness changes in their vicinity can affect grounding-line ice flux over large distances. We find, for example, that the shelf areas around Berkner Island—the ice rise separating Filchner and Ronne ice shelves—influence the entire upstream region. In contrast to ice rises, where the ice flow is almost stagnant, ice rumples, such as Doake Ice Rumples, are smaller obstacles across which the ice shelf slides. In general, ice-shelf thinning applied around ice rumples has a greater impact on grounding line flux than thinning around ice rises (compare Fig. 1b and c).

Yet, other regions have very limited impacts on ice flux. Such 'passive' ice shelf regions are not only found near calving fronts but also close to grounding lines (white shelf areas in Fig. 1), that is, in areas that might be expected to be highly buttressed and located well upstream of the 'safety band' of Antarctic ice shelves[22]. Two examples of such areas are the regions directly downstream of the grounding line of Filchner Ice Shelf between Support Force and Foundation ice streams (Fig. 1c) and downstream of Kamb Ice Stream (Fig. 1b). Consistently, these areas have lower buttressing values compared to their surroundings[22] (but higher than the passive shelf areas) and for the regions with higher buttressing values in the middle of Ronne and Ross ice shelves we find significant grounding line flux responses as well.

Ice-shelf buttressing affects the stresses along the grounding lines, and with them the horizontal spreading rate of the grounded ice upstream. The response in ice velocity at the grounding line, and therefore in ice flux quantified here, is the integrated effect of changes in spreading rate upstream from the grounding line. Therefore, unless these changes extend over a substantial distance, the impact on grounding line ice flux will be limited. It follows that the changes in ice flux are not only a direct function of perturbation in stresses at the grounding line, but are also strongly affected by mechanical conditions upstream of the grounding line and in particular by the length-scale of stress transmission. The latter is primarily determined by the slip ratio, that is, the ratio of basal sliding to internal ice deformational velocity and ice-stream width[32]. Over ice shelves, the sliding ratio is infinite and the stress-transmission length scale unbounded. However, this does not imply that ice-thickness changes at one location within an ice shelf will necessarily have a wide impact on flow. Changes in ice thickness of an unbuttressed ice shelf have, for example, no impact on upstream flow. It is therefore the interplay between the applied thinning, degree of drag provided by ice shelf margins and pinning points, as well as the mechanical basal conditions upstream of the grounding line that determines the flux response at the grounding line. This is reflected in the complex response pattern that we find for locally applied thinning in Antarctic ice shelves.

While perturbations downstream of fast-moving ice streams generally induce a local acceleration of ice flow (an example of this feature for Pine Island Glacier is given in Fig. 2a), our results show that the effect of ice-shelf thinning can reach over long distances: thinning near Ross Island, for example, induces immediate speed changes that reach across the entire ice shelf, accelerating

© 2017 Macmillan Publishers Limited, part of Springer Nature. All rights reserved.

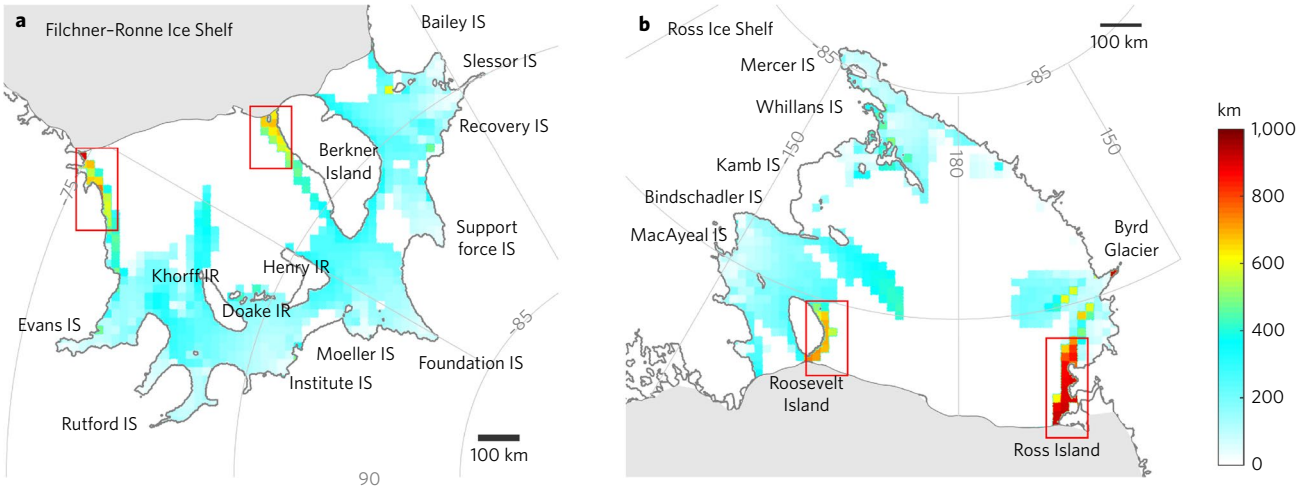

Fig. 3 | Tele-buttressing. a,**b**, The maximal response distance for every perturbation location of Filchner–Ronne (**a**) and Ross (**b**) Ice Shelf. The maximal response distance is defined as the maximum distance for which the remote buttressing flux response number, that is, the response ratio over all grounding lines that are farther away than this distance, is greater than a threshold of 0.02%. Ocean is shown in grey.

Bindschadler and MacAyeal ice streams located more than 900 km away (Fig. 2b).

This 'tele-buttressing' effect can be observed in several regions. Fig. 3 shows the maximal response distance for each location in the Ross and Filchner–Ronne ice shelves in contrast to the overall response strength given in Fig. 1b,c. In both ice shelves, we find several critical regions (indicated by red boxes) where local perturbation affects remote grounding lines, often across streamlines of the ice shelf flow. The direction of these teleconnections can be derived from interaction matrices (such as the ones given in Supplementary Figs. 3, 4), which record the response pattern for each perturbation area. Tele-buttressing regions with especially far-reaching effects in Filchner–Ronne Ice Shelf are the west coast of Ronne Ice Shelf and the west coast of Berkner Island.

It is well-understood that changes in mechanical contact between ice shelves and ice-shelf pinning points can affect ice shelf flow[1]. Our analysis shows how thinning of ice shelves—involving no reduction in grounded areas or loss of mechanical contact between floating and grounded sections—affects the flux across grounding lines. In contrast to the direct loss of pinning points, where the resulting stress perturbations are generally felt over whole ice shelves, the impact of a local modification in ice shelf thickness on ice flow is arguably more complicated, as the range over which such a perturbation acts depends on the large-scale geometry of the specific ice shelf. Whereas non-locality of ice-shelf thinning follows from the general characteristics of the elliptical system of equations describing the vertically integrated momentum balance in ice shelves and ice streams[30,31,33,34], the range of the response over some hundreds of kilometres from the source in the tele-buttressing areas, which we identify here, has not been quantified before.

Our approach is purely diagnostic and does not encompass future projections of grounding line flux, however, it serves to map out the most critical regions within Antarctic ice shelves that can induce a strong response—in either magnitude or distance or both—of the grounded ice to even slight changes in ice shelf thickness. The immediate flux response derived here is independent of observed thinning patterns, which allows our results to be transferred to any observed or possible changes in ice shelf thickness in the near future, for example, changes owing to local alterations in the ocean circulation. Shifts in the position of the thermocline can be expected to affect the melting of ice near grounding lines the most, where ice thicknesses are greatest[35,36]. Because these areas are also the most critical regions found in our analysis, the overall ice discharge is especially sensitive to changes in ocean circulation. Currently, the ice shelves in the Amundsen Region, which might be undergoing unstable retreat[37–39], experience the highest thinning rates (on average 19.4 metres per decade with a maximum of 66.5 metres per decade[4]) near their grounding lines. Our analysis shows that the flux response for these shelves is particularly high. Should oceanic circulations underneath Antarctic ice shelves change in the future (as projected for higher greenhouse gas emission scenarios for instance in the Weddell Sea[10]), other critical shelf regions might increasingly melt and trigger additional grounded ice loss. The critical shelf regions identified here should therefore be monitored with particular care because changes in the ambient ocean water or surrounding atmosphere and subsequent thinning in these areas can have an impact far beyond expected local effects.

Methods

Methods, including statements of data availability and any associated accession codes and references, are available at https://doi.org/10.1038/s41558-017-0020-x.

Received: 27 June 2017; Accepted: 8 November 2017;
Published online: 11 December 2017

References

1. Thomas, R. H. The creep of ice shelves: interpretation of observed behaviour. *J. Glaciol.* **12**, 55–70 (1973).
2. Hughes, T. Is the west Antarctic Ice Sheet disintegrating? *J. Geophys. Res.* **78**, 7884–7910 (1973).
3. Dupont, T. K. & Alley, R. B. Assessment of the importance of ice-shelf buttressing to ice-sheet flow. *Geophys. Res. Lett.* **32**, L04503 (2005).
4. Paolo, F. S., Fricker, H. A. & Padman, L. Volume loss from Antarctic ice shelves is accelerating. *Science* **348**, 327–331 (2015).
5. Bindschadler, R. A. Hitting the ice sheets where it hurts. *Science* **311**, 1720–1721 (2006).
6. Pritchard, H. D. et al. Antarctic ice-sheet loss driven by basal melting of ice shelves. *Nature* **484**, 502–505 (2012).
7. Wouters, B. et al. Dynamic thinning of glaciers on the Southern Antarctic Peninsula. *Science* **348**, 899–903 (2015).
8. Rott, H., Rack, W., Skvarca, P. & De Angelis, H. Northern Larsen Ice Shelf, Antarctica: further retreat after collapse. *Ann. Glaciol.* **34**, 277–282 (2002).
9. De Angelis, H. & Skvarca, P. Glacier surge after ice shelf collapse. *Science* **299**, 1560–1562 (2003).
10. Hellmer, H. H., Kauker, F., Timmermann, R., Determann, J. & Rae, J. Twenty-first-century warming of a large Antarctic ice-shelf cavity by a redirected coastal current. *Nature* **485**, 225–228 (2012).
11. Rignot, E., Jacobs, S., Mouginot, J. & Scheuchl, B. Ice-shelf melting around Antarctica. *Science* **341**, 266–270 (2013).

© 2017 Macmillan Publishers Limited, part of Springer Nature. All rights reserved.

12. Dutrieux, P. et al. Strong sensitivity of Pine Island ice-shelf melting to climatic variability. *Science* **343**, 174–178 (2014).
13. Church, J. A. et al. in *Climate Change 2013: The Physical Science Basis.* Ch. 13 (eds Stocker, T. F. et al.) 1137–1216 (Cambridge Univ. Press, Cambridge, UK, 2013).
14. Mercer, J. H. West Antarctic ice sheet and CO_2 greenhouse effect: a threat of disaster. *Nature* **271**, 321–325 (1978).
15. Bindschadler, R. A. et al. Ice-sheet model sensitivities to environmental forcing and their use in projecting future sea level (the SeaRISE project). *J. Glaciol.* **59**, 195–224 (2013).
16. Nowicki, S. et al. Insights into spatial sensitivities of ice mass response to environmental change from the SeaRISE ice sheet modeling project I: Antarctica. *J. Geophys. Res.* **118**, 1002–1024 (2013).
17. Levermann, A. et al. Projecting Antarctic ice discharge using response functions from SeaRISE ice-sheet models. *Earth Syst. Dyn.* **5**, 271–293 (2014).
18. Lenaerts, J. T. M. et al. Meltwater produced by wind–albedo interaction stored in an East Antarctic ice shelf. *Nat. Clim. Change* **7**, 58–62 (2016).
19. Depoorter, M. A. et al. Calving fluxes and basal melt rates of Antarctic ice shelves. *Nature* **502**, 89–92 (2013).
20. Holland, D. M., Thomas, R. H., de Young, B., Ribergaard, M. H. & Lyberth, B. Acceleration of Jakobshavn Isbræ triggered by warm subsurface ocean waters. *Nat. Geosci.* **1**, 659–664 (2008).
21. Fürst, J. J. et al. Assimilation of Antarctic velocity observations provides evidence for uncharted pinning points. *Cryosphere* **9**, 1427–1443 (2015).
22. Fürst, J. J. et al. The safety band of Antarctic ice shelves. *Nat. Clim. Change* **6**, 479–482 (2016).
23. Gudmundsson, G. H., Krug, J., Durand, G., Favier, L. & Gagliardini, O. The stability of grounding lines on retrograde slopes. *Cryosphere* **6**, 1497–1505 (2012).
24. Goldberg, D., Holland, D. M. & Schoof, C. Grounding line movement and ice shelf buttressing in marine ice sheets. *J. Geophys. Res.* **114**, F04026 (2009).
25. Gudmundsson, G. H. Ice-shelf buttressing and the stability of marine ice sheets. *Cryosphere* **7**, 647–655 (2013).
26. Gagliardini, O., Durand, G., Zwinger, T., Hindmarsh, R. C. A. & Le Meur, E. Coupling of ice-shelf melting and buttressing is a key process in ice-sheets dynamics. *Geophys. Res. Lett.* **37**, L14501 (2010).
27. Matsuoka, K. et al. Antarctic ice rises and rumples: their properties and significance for ice-sheet dynamics and evolution. *Earth Sci. Rev.* **150**, 724–745 (2015).
28. Fretwell, P. et al. Bedmap2: Improved ice bed, surface and thickness datasets for Antarctica. *Cryosphere* **7**, 375–393 (2013).
29. Rignot, E., Mouginot, J. & Scheuchl, B. Ice flow of the Antarctic ice sheet. *Science* **333**, 1427–1430 (2011).
30. Morland, L. Unconfined ice shelf flow. 99–116 *Proc. Workshop Dynamics West Antarctic Ice Sheet* (eds van der Veen, C. J. & Oerlemans, J.) (Reidel, 1987).
31. MacAyeal, D. R. Large-scale ice flow over a viscous basal sediment: theory and application to ice stream B, Antarctica. *J. Geophys. Res.* **94**, 4071–4087 (1989).
32. Gudmundsson, G. H. Transmission of basal variability to a glacier surface. *J. Geophys. Res.* **108**, 2253 (2003).
33. Weis, M., Greve, R. & Hutter, K. Theory of shallow ice shelves. *Contin. Mech. Thermodyn.* **11**, 15–50 (1999).
34. Schoof, C. Ice sheet grounding line dynamics: steady states, stability, and hysteresis. *J. Geophys. Res.* **112**, F03S28 (2007).
35. Jenkins, A. et al. Decadal ocean forcing and Antarctic ice sheet response: lessons from the Amundsen Sea. *Oceanography* **29**, 106–117 (2016).
36. Turner, J. et al. Atmosphere–ocean–ice interactions in the Amundsen Sea Embayment, West Antarctica. *Rev. Geophys.* **55**, 235–276 (2017).
37. Joughin, I., Smith, B. E. & Medley, B. Marine ice sheet collapse potentially under way for the Thwaites Glacier Basin, West Antarctica. *Science* **334**, 735–738 (2014).
38. Favier, L. et al. Retreat of Pine Island Glacier controlled by marine ice-sheet instability. *Nat. Clim. Change* **4**, 117–121 (2014).
39. Rignot, E., Mouginot, J., Morlighem, M., Seroussi, H. & Scheuchl, B. Widespread, rapid grounding line retreat of Pine Island, Thwaites, Smith, and Kohler glaciers, West Antarctica, from 1992 to 2011. *Geophys. Res. Lett.* **41**, 3502–3509 (2014).

Acknowledgements

This research has received funding from the Deutsche Forschungsgemeinschaft (DFG) grant number LE 1448/8-1, from COMNAP Antarctic Research Fellowship 2016, the German Academic National Foundation, Evangelisches Studienwerk Villigst and from the NERC NE/L013770 Large Grant 'Ice shelves in a warming world: Filchner Ice Shelf system, Antarctica'.

Author contributions

R.R., G.H.G., A.L. and R.W. designed the research and contributed to the analysis. R.W. conceived the study. G.H.G. developed the Úa model and created the Antarctica setup. R.R. carried out the analysis. R.R., G.H.G. and R.W. wrote the manuscript.

Competing interests

The authors declare no competing financial interests.

Additional information

Supplementary information is available for this paper at https://doi.org/10.1038/s41558-017-0020-x.

Reprints and permissions information is available at www.nature.com/reprints.

Correspondence and requests for materials should be addressed to R.W.

Publisher's note: Springer Nature remains neutral with regard to jurisdictional claims in published maps and institutional affiliations.

© 2017 Macmillan Publishers Limited, part of Springer Nature. All rights reserved.

Methods

Ice-sheet model. The experiments are conducted with the ice dynamics model Úa, which has been used successfully to study ice-shelf ice-stream systems for both idealized setups[23,25,40] and realistic, more complex geometries[38,41]. Úa is a finite-element model that uses unstructured grids and enables localized grid refinement in the vicinity of grounding lines. Here the model is used to solve the shallow-shelf/shelfy-stream approximation (see for example, refs [31,42]) using Glen's flow law with a stress exponent $n=3$, and a non-linear Weertman-type sliding law with stress exponent $m=3$. In all calculations presented here triangular six-node elements with quadratic base functions were used. The Antarctic-wide mesh (generated with Gmsh[43]) consists of 544,801 elements and 1,097,274 nodes and is refined in the vicinity of the grounding line. The elements have a maximum size of 120,387 m in the interior of the continent and minimum size of 383 m along the grounding line. Mean element size is 4,901 m and median 3,907 m.

Model initialization. Modelling parameters related to basal conditions and ice rheology are the basal slipperiness, C (Supplementary Fig. 5) and the ice-rate factor, A (Supplementary Fig. 6). We initialized the ice-flow model by changing the ice-rate factor and basal slipperiness using an inverse model methodology until the surface velocities of the numerical model closely matched the measurements of ice flow in the MEaSUREs surface velocities based on the Bedmap2 ice thickness and bed geometry estimates[28,29]. We used a Bayesian inversion that was constrained by a priori knowledge about A and C expressed through corresponding covariance matrices generated by an exponential covariance functions. The average difference between modelled and observed ice speed is 43.8 metres per year with a median of 17.7 metres per year and a root mean square error of 93.8 metres per year. The ice-rate factor- and basal slipperiness-derived distributions can be obtained from the Polar Data Centre (http://doi.org/bndr). Weakening of the effective viscosity due to bending stresses in the vicinity of the grounding line, which is not included in the shallow-shelf/shelfy-stream approximation[44], will be indirectly accounted for in the inverted ice-rate factor.

Vertically averaged ice densities are calculated using firn thickness fields from RACMO2[45], assuming a constant ice density of 910 kg m^{-3} and a firn density of 500 kg m^{-3}. The grounding line position is determined by the flotation criterion (Supplementary Fig. 7). While some pinning points are missing in Bedmap2[21], our main focus lies on Filchner–Ronne and Ross Ice Shelves, where Bedmap2 data includes the most important obstacles. Computed grounding line fluxes for present-day Antarctica agree reasonably well with observations, with a tendency for most ice shelves to have slightly lower modelled than observed fluxes[29], see Supplementary Table 1.

Thinning experiments. Based on inverted ice softness and basal friction fields, ice velocities are computed: first for the unperturbed state that corresponds to the current state of Antarctica (Supplementary Fig. 7), then applying local perturbations to the ice thickness. We use an Antarctic wide, regular perturbation grid of 20 km × 20 km resolution (in polar stereographic projection) that has 275 × 220 grid cells. Each cell of this perturbation grid therefore contains a multitude of nodes of the unstructured Úa grid (see Supplementary Fig. 8). For each perturbation cell, instantaneous velocity changes are computed by solving the shallow-shelf/shelfy-stream approximation[31] for a thickness perturbation of 1 m at all its floating nodes. All nodes belonging to elements that contain parts of the grounding line are excluded. This ensures that the model response is only due to thinning-induced changes in the stress field and that potential effects of changes in driving stress over grounded regions are excluded. Because the ice thickness at the grounding line is not affected by the experiments, we can derive the immediate changes of the flux across the grounding line from the velocity changes in the experiments. For each perturbation experiment, velocities are computed for the entire Antarctic setup.

Interaction matrix and grounding line flux response. For all elements of the perturbation grid, we obtain an interaction matrix as given for Filchner–Ronne and Ross Ice Shelves in Supplementary Figs. 3 and 4, respectively. Its pr-th entry is the change in grounding line flux caused by a perturbation in square p that is integrated over the parts of the grounding line within square r:

$$I_{(\mathrm{p,r})} = \int_{x \in GL(r)} \Delta Q_p(\mathrm{x})\mathrm{dl} \tag{1}$$

where p is the perturbed square and r the response square containing the grounding line section GL(r). The local change in flux at the grounding line at position x caused by a perturbation in p is $\Delta Q_p(x)$.We do not account for changes in flux across the grounding lines of ice rises or rumples. Note that for squares of the perturbation grid that do not contain grounding line sections, the entries in the interaction matrix are zero. Summing the elements of the interaction matrix over one column p yields the continent-wide response in flux across the grounding line that a perturbation in square p causes.

Buttressing flux response number. The ratio of the immediate grounding line flux change to the externally induced ice-shelf thinning is defined as the buttressing flux response number θ_B. The buttressing flux response number at a node x within square p is given by

$$\theta_B(x) = R/P \tag{2}$$

where P is the perturbation strength for square p and R is the response in flux integrated over all grounding lines. The latter is equivalent to the sum of all elements in the pth column of the interaction matrix. Note that θ_B at each location within an ice shelf is calculated by adding up the total perturbation in ice flux over the whole ice shelf, and in cases where an ice shelf has several separated grounding lines, the contribution of all those grounding lines are included. While the response is integrated over all grounding lines of the Antarctic-wide setup, a change in flux occurs only in the ice shelf where the perturbation was applied (see for example, Fig. 2). Here, the buttressing flux response number is calculated by multiplying the instantaneous perturbation in flux across grounding lines by a time interval of one year. The buttressing flux response number can equally well be thought of as representing a rate of mass loss (with units per year). A perturbation of 2 m over area A at position x, for example, increases the flux across the grounding line by $2 \times A \times \theta_B(x)$ Gt per year, assuming that the ice flux responds linearly to the perturbations as further discussed below (see also Supplementary Fig. 2). A buttressing flux response number of 100% indicates that the entire ice mass taken from the ice shelf by the perturbation translates (via a reduction of buttressing and a resulting acceleration of ice flow) into an equivalent additional mass loss from the ice sheet within one year (given fixed boundary conditions).

Tele-buttressing. To account for remote grounding line flux responses, we introduce the notion of tele-buttressing. To this end, we define the maximal response distance for a perturbation cell p as the maximum distance such that the remote buttressing response ratio (along the grounding line parts that are at least at that distance from the perturbation location) is greater than a threshold t:

$$d_p = \max\left\{ \mathrm{r} > 0 \left| \int_{|x - x(p)| > r} \Delta Q_p(x)\mathrm{dl} > t \right. \right\} \tag{3}$$

where $x(p)$ is the position of the cell p. We set the threshold to $t = 0.02\%$. Thinning along the margins of a confined ice shelf will almost invariably affect buttressing along all grounding lines, and although the resulting impact at any given location along the grounding line might be small, the cumulative impact across the whole grounding line can be comparable to or larger than the impact of the same amount of thinning applied locally directly downstream of a grounding line.

Uniform perturbation experiments. In an additional set of experiments, we thin the entire ice shelves uniformly by 1 m. The results from these experiments are given in Supplementary Table 1. With these experiments, we diagnose the immediate response of the grounding line flux to uniform perturbations of the entire ice shelf. Realistic thinning patterns are not uniform, but these idealized uniform perturbation experiments allow us to investigate the additivity of the transfer functions (discussed in 'Linearity range of grounding line flux response') and to identify the relative importance of individual ice shelves to global sea-level change. As expected, the large Filchner–Ronne Ice Shelf and Ross Ice Shelf show the highest total response with, respectively, 1.07 Gt per year and 0.79 Gt per year flux increase to an abrupt 1-metre thinning of the floating ice. Relative to their area, small ice shelves, however, have a comparably high impact (consistent with results using simplified geometries, see for example, ref. [46]). The 1-metre thinning of the ice shelf adjacent to Pine Island Glacier, for example, increases the ice flux across the grounding line instantaneously by 0.285 Gt per year (Supplementary Table 1). These flux changes correspond to about 0.27% of the total current flux across Pine Island Glacier's grounding line. Note that the applied perturbations (of 1 m) are very small compared to the overall thickness of Antarctic ice shelves (in the order of 100 to 1,000 metres).

Linearity range of grounding line flux response. The range of linearity (additivity and homogeneity) of the immediate response in grounding line flux to thickness perturbations is numerically diagnosed: for all ice shelves listed in Supplementary Table 1, we find that adding the grounding line flux response of its perturbation squares compares well with the total shelf response, that is, the grounding line flux changes for a uniform perturbation of the corresponding ice shelf. Furthermore, Supplementary Fig. 2 shows that the uniform response scales with the perturbation up to a few metres. Our analysis can thus give insight into the expected response of the Antarctic Ice Sheet to currently observed ice-shelf thinning patterns.

Stress adjustment to local thinning. Our ice flow model Úa solves the shallow-shelf/shelfy-stream approximation of the momentum balance describing ice

© 2017 Macmillan Publishers Limited, part of Springer Nature. All rights reserved.

shelf flow and flow of fast-moving ice streams[31,42]. In an ice shelf, horizontal 'membrane' stress gradients balance the body force[47]. For the flowline case of an ice shelf, the longitudinal 'membrane stresses' are a local function of ice thickness[48]. Therefore, in an ice shelf with a complicated geometry varying in two horizontal dimensions, stresses will likewise be affected by changes in ice thickness. As the shallow-shelf/shelfy-stream approximation is an elliptic equation that is non-local in the sense that any solution of the system will not only depend on local properties but also on boundary conditions and the properties of the surrounding ice, a local perturbation has the potential to affect far-off ice flow by changing the stress field within the ice shelf and at the grounding lines. This is reflected by the fact that stresses within an ice shelf are transmitted immediately across the entire ice shelf as there is no basal resistance felt by the ice shelf at its base. Relevant for this is the transmission of horizontal stresses which are fully included in the shallow-shelf/shelfy-stream approximation. The experiments conducted here are hence sufficient to quantify the effect of a buttressing reduction on the ice flow at the grounding line. They further enable disentangling the effect of buttressing from further mechanisms and feedbacks that would control grounding line movement and stability in a prognostic model run.

Code availability. The scripts that support the findings of this study are available from the corresponding authors upon request.

Data availability. The data that support the findings of this study are available from the corresponding authors upon request.

References

40. Pattyn, F. et al. Grounding-line migration in plan-view marine ice-sheet models: results of the ice2sea MISMIP3d intercomparison. *J. Glaciol.* **59**, 410–422 (2013).
41. De Rydt, J., Gudmundsson, G. H., Rott, H. & Bamber, J. L. Modeling the instantaneous response of glaciers after the collapse of the Larsen B Ice Shelf. *Geophys. Res. Lett.* **42**, 5355–5363 (2015).
42. Hutter, K. *Theoretical Glaciology: Material Science of Ice and the Mechanics of Glaciers and Ice Sheets* (D. Reidel Publishing Company, Tokyo, Terra Scientific Publishing Company, 1983).
43. Geuzaine, C. & Remacle, J.-F. Gmsh: a 3-D finite element mesh generator with built-in pre- and post-processing facilities. *Int. J. Numer. Methods Eng.* **79**, 1309–1331 (2009).
44. Pattyn, F. et al. Results of the marine ice sheet model intercomparison project, MISMIP. *The Cryosphere* **6**, 573–588 (2012).
45. Lenaerts, J. T. M., van den Broeke, M. R., van de Berg, W. J., van Meijgaard, E. & Kuipers Munneke, P. A new, high-resolution surface mass balance map of Antarctica (1979–2010) based on regional atmospheric climate modeling. *Geophys. Res. Lett.* **39**, L04501 (2012).
46. Dupont, T. K. & Alley, R. B. Role of small ice shelves in sea-level rise. *Geophys. Res. Lett.* **33**, L09503 (2006).
47. Hindmarsh, R. C. A. The role of membrane-like stresses in determining the stability and sensitivity of the Antarctic ice sheets: back pressure and grounding line motion. *Phil. Trans. R. Soc. A* **364**, 1733–1767 (2006).
48. Weertman, J. Deformation of floating ice shelves. *J. Glaciology* **3**, 38–42 (1957).

© 2017 Macmillan Publishers Limited, part of Springer Nature. All rights reserved.